Effect of nanodiamond fluorination on the efficiency of quasispecular reflection of cold neutrons

V. V. Nesvizhevsky,[1,*] M. Dubois,[2] Ph. Gutfreund,[1] E. V. Lychagin,[3] A. Yu. Nezvanov,[1,4,5] and K. N. Zhernenkov[1,3]

[1]*Institut Max von Laue–Paul Langevin, 71 avenue des Martyrs, Grenoble, F-38042, France*

[2]*ICCF, Université Clermont Auvergne, 49 boulevard François-Mitterrand, Clermont-Ferrand, F-60032, France*

[3]*Joint Institute for Nuclear Research, 6 Joliot Curie, Dubna, Ru-141980, Russia*

[4]*Universite Grenoble-Alpes, 621 avenue Centrale, Saint-Martin-d'Hères, F-38400, France*

[5]*Moscow Polytechnic University, 38 Bolshaya Semenovskaya street, Moscow, Ru-107023, Russia*

(Received 11 January 2018; revised manuscript received 31 January 2018; published 21 February 2018)

Nanomaterials, which show large reflectivity for external radiation, are of general interest in science and technology. We report a result from our ongoing research on the reflection of low-energy neutrons from powders of detonation diamond nanoparticles. Our previous work showed a large probability for quasispecular reflection of neutrons from this medium. The model of neutron scattering from nanoparticles, which we have developed, suggests two ways to increase the quasispecular reflection probability: (1) the reduction of incoherent scattering by substitution of hydrogen with fluorine inside the nanoparticles, and (2) the sharpening of the neutron optical potential step by removal of amorphous sp^2 carbon from the nanoparticle shells. We present experimental results on scattering of slow neutrons from both raw and fluorinated diamond nanoparticles with amorphous sp^2 carbon removed by gas-solid fluorination. These results show a clear increase in quasispecular reflection probability.

DOI: 10.1103/PhysRevA.97.023629

I. INTRODUCTION

Scattering of waves in disordered media is an important topic in many domains of science [1]. When the typical size d of the scatterer inhomogeneities is much larger than the radiation wavelength λ, the wave is scattered at individual inhomogeneities to small angles of the order of

$$\vartheta_{\text{eff}} \sim \frac{\lambda}{d}. \tag{1}$$

ϑ_{eff} is often called the effective small-angle scattering angle; the exact form of the angular dependence of the scattering depends on the specific nature of the scattering process.

Such scattering, in particular neutron scattering on inhomogeneities of the neutron-nuclei optical potential of matter, is a powerful method [2–5] for studying the sizes, shapes, and positions of scatterers in matter. Usually, in a classical small-angle scattering experiment the scattering pattern is recorded after transition through the sample.

However, waves incident on the boundary of a disordered medium at small angles can also be reflected because of multiple small-angle scattering events. Examples are the reflection of electromagnetic waves from atmospheric inhomogeneities, aerosols, rain, snow, biological issues, composite materials, etc. [6]. Charged particles (protons, electrons) or neutral particles (atoms) provide other examples of wave reflection from disordered media. All these and other analogous processes obey the general laws. The most probable angle of reflection and the spread of the reflection angles are equal to the angle of incidence, and the probability of such reflection is quite large at certain conditions. For any type of radiation with a given wavelength and scatterers with a given size, the probability of such reflection depends on the angular properties of the scattering and the ratio of the elastic small-angle scattering probability to the probability of losses, defined accordingly to the specific physical process. Reference [7] describes them analytically in a general form.

Following this analogy, we found that powders of detonation nanodiamonds [8,9] (DNDs) with typical sizes of nanoparticles of 4–5 nm reflect cold neutrons (CNs) quasispecularly at small incident angles [10,11]. They reflect very cold neutrons (VCNs) diffusively at any incidence angle [12–16]. CNs are loosely defined as neutrons extracted with reasonable intensities from cryogenic neutron sources installed in the vicinity of the core of a nuclear reactor or a spallation source; the typical wavelengths of CNs are 0.4–2.5 nm (the velocities are 160–1000 m/s; the energies are 0.13–5.1 meV). The VCN wavelengths range from the maximum wavelength of CNs to the minimum wavelength of ultracold neutrons (UCNs); the typical wavelengths of VCNs are 2.5–60 nm (the velocities are 7–160 m/s; the energies are 0.25–130 μeV). UCNs, in turn, have an interesting property of total reflection from the optical potential at any incident angle. In both cases (quasispecular and diffusive reflection), DNDs have provided a record reflectivity due to the exceptional combination of the high coherent scattering length of carbon ($b^{\text{C}}_{\text{c.sc.}} = 6.65$ fm) (the corresponding coherent scattering cross section $\sigma^{\text{C}}_{\text{c.sc.}} = 5.55b$)' high volume density of diamond, 3.5 g/cm^3; and low neutron losses [the absorption cross section $\sigma^{\text{C}}_{\text{abs}} = 3.5$ mb and relatively low inelastic scattering cross section (the value depends on the temperature)]; and also their availability in close-to-optimum sizes ($\sim 2-10$ nm). The geometrical sizes and shapes [17] of nanoparticles are important for optimizing the specific properties of such neutron reflectors, which in turn depend on specific applications [18,19]; this is work that still needs to be done in most cases.

*nesvizhevsky@ill.eu

As we can conclude from Ref. [7] in application to a neutron, the efficiency of reflection is a function of the ratio of the elastic small-angle scattering cross section $\sigma_{\text{c.sc.}}$ to the cross section σ_{loss} of all other processes equivalent to losses, since they reduce the radiation flux in quasispecular directions. For a neutron, this cross section includes nuclear absorption, incoherent, Bragg, and inelastic scattering:

$$\sigma_{\text{loss}} = \sigma_{\text{abs}} + \sigma_{\text{inc.sc.}} + \sigma_{\text{Bragg}} + \sigma_{\text{inel.sc.}}. \tag{2}$$

Here we assume that inelastic scattering rejects the neutron by scattering to a large angle. We do not also consider the interference of neutron scattering on (a) the optical potential and on (b) the diamond crystal lattice. The last simplification is incorrect at neutron wavelengths comparable to the lattice spacing. This interference is insignificant at large wavelengths, but is of interest for characterizing nanopowders at small wavelengths. We will consider this possibility in another work.

Thus the efficiency of quasispecular scattering is determined by the ratio

$$\varepsilon = \frac{\sigma_{\text{c.sc.}}}{\sigma_{\text{loss}}}. \tag{3}$$

To select conditions that enhance the efficiency of quasispecular reflection of neutrons, we have to know the values of σ_{loss} and $\sigma_{\text{c.sc.}}$. The calculation of σ_{loss} is straightforward. For calculating $\sigma_{\text{c.sc.}}$, we used a simplistic formalism that involves the interaction of a neutron with the optical potential of a single nanoparticle in the first Born approximation, and analyzed other processes as perturbations. The amplitude for a neutron with the energy $(\hbar k)^2/(2m)$, with $\hbar$ the reduced Planck constant, k the neutron wave vector. and m the neutron mass, to be scattered at a spherical nanoparticle with the radius r and the optical potential V, at an angle of θ, is equal to

$$f(\theta) = -\frac{2m}{\hbar^2} V R^3 \left[\frac{\sin(qr)}{(qr)^3} - \frac{\cos(qr)}{(qr)^2}\right], \tag{4}$$

where $q = 2k\sin(\theta)$ is the momentum transfer. The function f is called the scattering function.

The total elastic cross section is

$$\sigma_{\text{c.sc.}} = \int |f|^2 d\Omega = 2\pi \left|\frac{2m}{\hbar^2} V\right|^2 r^6 \frac{1}{(kr)^2} I(kr), \tag{5}$$

where $I(kr) = \frac{1}{4}[1 - \frac{1}{(2kr)^2} + \frac{\sin(4kr)}{(2kr)^3} - \frac{\sin^2(2kr)}{(2kr)^4}]$.

In the earlier experiments [20], hydrogen (H) in DNDs was an important cause of neutron loss, which reduces the efficiency of quasispecular reflection [see Eq. (3)]. H is present in raw DNDs in large quantities (on average one H atom per 7.4 ± 0.2 C atoms), and has a large absorption cross section ($0.33b$) and an exceptionally large incoherent scattering cross section ($108 \pm 2b$ at room temperature). Another drawback of previous experiments was the presence of amorphous sp^2 carbon in nanoparticle shells, which smeared out the particle shape and thus reduced the amplitude of the scattering function [see Eqs. (3) and (5)]. Thus removing H from DNDs and sharpening the nanoparticle form, due to the removal of amorphous sp^2 C shells, is expected to increase the efficiency of neutron reflection. Recently, we applied a chemical treatment to the nanodiamonds for achieving this goal: gas (F_2)-solid fluorination [21]. In the present article, we explore experimentally the effect of DND fluorination on the efficiency of quasispecular reflection of cold neutrons. This research is part of the SLOw Neutron reflectors (SLON) collaboration.

The method of neutron reflectivity measurements is analogous to that used in Refs. [10,11]. However, the plane of the surface of the sample is prepared with higher accuracy, so the angular and velocity resolution is higher and the systematic effects are smaller.

We describe samples in Sec. II, experimental methods in Sec. III, experimental results in Sec. IV, and computer simulations in Sec. V.

II. SAMPLES

In order to assess the effect of the fluorination of nanodiamonds on the efficiency of quasispecular reflection of cold neutrons, we compared directly samples of raw DNDs and fluorinated DNDs (F-DNDs) [21] of the same type as used in Refs. [10,11]. DNDs were produced at the institute RFNC-VNIITF (Snezhinsk) in accordance with the procedure described in Technical Regulations act TY 2-037-677-94. The average size of the diamond nanoparticle cores, measured by x-ray diffraction, is 4.3 nm [21]. Sizes range from $\sim$2 to $\sim$10 nm. Note that a distribution of nanoparticle sizes affects the probability of quasispecular reflection to a smaller extent than a mean value does.

The container and conditions for preparation of the sample differ from those used in the previous experiment; we explain the motivation below.

The inset in Fig. 1 shows a sample in the sample container. The container is made of aluminum (Al). Its external sizes are $110 \times 50 \times 10\,\text{mm}^3$. The size of the volume filled with DNDs (F-DNDs) is $100 \times 40 \times 6\,\text{mm}^3$. A thin silicon (Si) window (a wafer) covers the container surface exposed to neutrons. The window thickness is 180 μm. We selected the window material and thickness so that neutron losses in the window are limited and simultaneously the window is rigid enough to provide its flatness. The density of DND and F-DND samples is $0.29-0.30\,\text{g/cm}^3$. Important differences between the sample's containers used in Refs. [10,11] and those used in the present work are the following: (a) A well-polished highly flat Si window defines the sample surface much better than a stretched Al foil did in the previous study. (b) The sample's depth is significantly smaller than that in the previous study which allows direct monitoring of the fraction of neutrons passing through the powder. Note that the sample mass of 7 g is $\sim$17 times smaller than the mass of the sample used in the previous study. This decrease in the mass of the sample does not reduce the probability of quasispecular reflection in the relevant velocity range but makes the method more accessible for practical applications.

The sample conditioning reproduces realistic experimental conditions of possible practical applications of the method. We had not evacuated the sample container and/or heated the sample in advance. Thus we allowed a possible adsorption of H-containing impurities from air and/or eventual chemical reactions with air on the surface of F-DNDs.

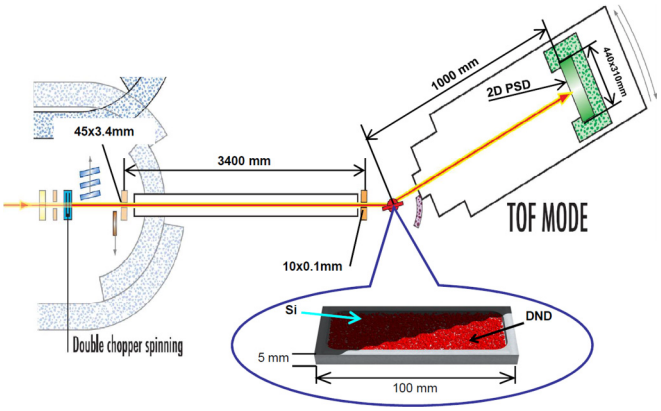

FIG. 1. A scheme (top view) of measurements of quasispecular reflection of cold neutrons from F-DNDs (DNDs) performed on the D17 instrument at ILL. The inset shows a sample of F-DNDs (DNDs) in the sample container: DND stands for diamond nanoparticles; the box indicates the sample container; Si indicates the window. The sharp end of the inset indicates the position of a sample installed on the translation-rotation stage. Neutrons arrive at the sample along the arrow from the liquid-deuterium cold neutron source in the ILL high-flux reactor (from left in the figure). A double chopper periodically interrupts the neutron beam, thus providing the time-of-flight measurements of the neutron spectrum. Various structures in front of the sample provide the suppression of unwanted beam-related backgrounds, neutron transport, and neutron beam collimation. Downstream of the sample, a two-dimensional position-sensitive ^{3}He detector (2D-PSD) within its shielding can move backward and forward inside the vacuum chamber, and/or rotate horizontally around the sample together with the vacuum chamber. An arrow downstream of the sample indicates schematically a neutron reflected quasispecularly from the sample.

III. EXPERIMENTAL METHOD

This study was performed using the neutron reflectometer D17 [22] at the ILL. We investigated the probability of quasispecular reflection as a function of the neutron wavelength ($\lambda\!\!\!^{-}_n$), incidence, and reflection angles.

As shown in Fig. 1, the D17's chopper periodically interrupts neutrons and thus allows measuring the neutron wavelength distributions using the time-of-flight method; the range of useful wavelengths extends from ∼1.6 to ∼27 Å.

A pair of standard D17 slits forms the spatial size and angular divergence of the neutron beam incident on a sample. The height and width of the second slit are equal to 10 and 0.1 mm, respectively, thus defining the beam size at a sample. The first slit of 155 mm in height and 3.4 mm in width, installed at 3.4 m upstream of the second one, defines the angular beam divergence of $\pm 5 \times 10^{-4}$ rad in the horizontal plane.

The D17 position-sensitive neutron detector records the reflection angle. The height and width of the neutron detector are 47 and 25 cm; the distance from a sample to the detector is 1 m. Some reflected neutrons miss the detector, as its vertical angular size might be smaller than the full range of vertical scattering angles; we will consider this effect in computer simulation in Sec. V.

The accuracy of setting (calibrating) all these parameters, as well as the neutron wavelength time-of-flight and detector position resolutions, are much better than the values relevant for quasispecular reflection.

The angle of neutron beam incidence to the sample surface (see Fig. 1) was set to 1°, 2°, and 3°, respectively. In each measurement, a sample was translated perpendicularly to the beam so that the beam entered the sample surface sharply close to its front edge. The scattering angle in the horizontal plane (see Fig. 1) is measured from the direction parallel to the sample surface. In order to cover a complete range of scattering angles, we set the detector to a number of angles and merged data sets.

A fraction of neutrons with sufficiently short wavelengths and incident at sufficiently large angles can penetrate through a sample or exit from its narrow side, due to the finite sample thickness and length. We monitored this effect in the position-sensitive detector.

The detector, when installed in the direct beam, measured the incident neutron flux as a function of the neutron wavelength; we used these data to calculate absolute probabilities. We measured the detector efficiency, as a function of position, with a water sample in the sample position; we used these data to correct for different efficiencies of neutron detection in different detector pixels.

We carried out all pairs of measurements, with DNDs and F-DNDs, respectively, in equivalent geometry with equivalent beam and spectrometer parameters; thus one can compare them directly, without any data treatment or/and computation.

IV. EXPERIMENTAL RESULTS

As mentioned above, the disadvantages associated with DNDs include the presence of H impurities and amorphous sp^2 C shells. Prompt-γ analysis showed [21] that the content of H in DNDs is drastically reduced by fluorination, achieving a level of 4 ppm, which is 35–60 times lower than that before fluorination. Solid state NMR, Raman, and Fourier-transform infrared spectroscopy (FTIR) proved that amorphous sp^2 carbon has been removed from the nanoparticle surface. Thus F-DNDs can be considered as practically pure and free of those impurities.

Standard two-dimensional representation of reflectometry data reveals an integral effect of the fluorination. Thus Fig. 2 shows the reflection probability of neutrons within the detector angular acceptance in comparative measurements with DND and F-DND samples in the geometry as indicated in Fig. 1 and described above.

First, note the sharp vertical line in Fig. 2 at a scattering angle of 1° equal to the angle of incidence. Specular reflection of neutrons from the surface of the thin Si window of the sample's container explains this line. On the one hand, its observation at long neutron wavelengths is quite useful for adjustments and calibrations. On the other hand, its contribution is small at shorter wavelengths, where there is the phenomenon of quasispecular reflection of cold neutrons from nanodiamond samples; thus one can subtract it, or correct for it, when needed.

As clear from Fig. 2, these two scattering patterns are similar to each other. The average scattering angle and the average spread of the scattering angles are approximately equal to the angle of incidence. However, the scattering probability is higher for F-DNDs than for DNDs.

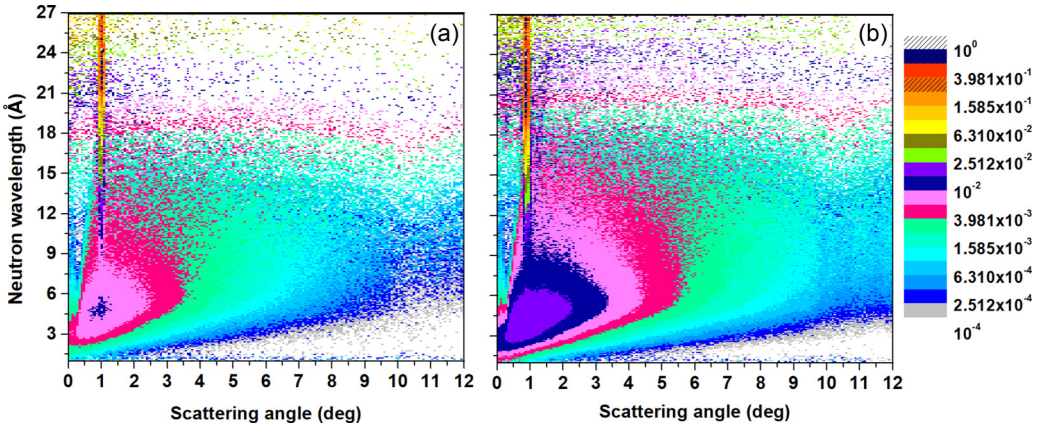

FIG. 2. The probability of neutron scattering from the surface of DND (on the left) and F-DND (on the right) powders as a function of the neutron wavelength (vertical axis, in angstroms) and the scattering angle (horizontal axis, in degrees). Different intensities and colors (in the inset on the right) indicate the relative number of neutrons measured in the detector. (a,b) correspond to the data measured with DNDs and F-DNDs, respectively. The neutron incidence angle is 1°.

In order to reveal regularities in these patterns, we integrated the data (a) over the scattering angle, and (b) over the neutron wavelength.

Figure 3 shows the result of the integration of the data presented in Fig. 2 over the whole range of scattering angles (note that the detector vertical size may be smaller than the vertical neutron spot size in the detector position; therefore the total probability of quasispecular reflection can be significantly larger than the values indicated in the figure). We compare the results for F-DNDs and DNDs for the incidence angles of 1°, 2°, and 3°, respectively.

All six experimental curves in Fig. 3 show similar general behavior.

The reflection efficiency is low at short wavelengths and increases with increasing wavelength. This is due to two factors:

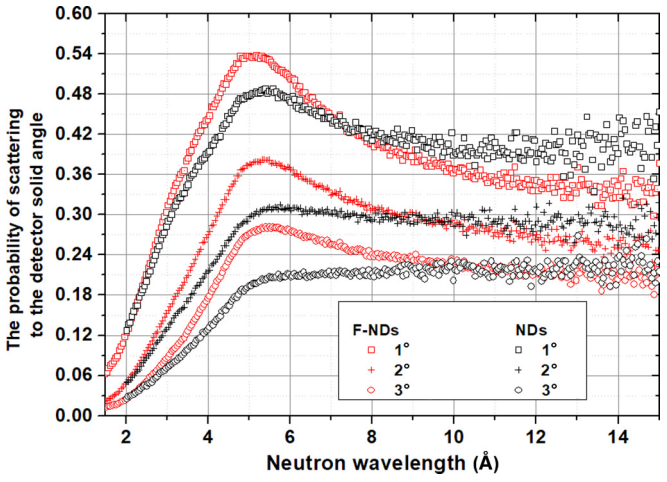

FIG. 3. Probability of neutron scattering, measured as a function of the neutron wavelength (horizontal axis, in angstroms) from F-DNDs (in red) and DNDs (in black) within the angular acceptance of the D17 detector in the geometry indicated in Fig. 1. We integrated the data over the whole range of scattering angles shown in Fig. 2, and normalized them to the total incident intensity. The incidence angle is 1°, 2°, and 3°, respectively, as indicated in the inset.

(a) Diffraction on the crystal lattice of the diamond cores of nanoparticles scatters neutrons to large angles, and thus eliminates them from quasispecular directions. The interplanar spacing in the diamond lattice is 3.57 Å. The finite dimensions of the nanoparticles broaden the diffraction peaks and reduce the diffraction efficiency. Thus the cutoffs are not sharp.

(b) Too small scattering angles at individual nanoparticles also suppress quasispecular reflection at too short wavelengths of ∼3 Å and below; this cutoff is not sharp as well due to the scatter of nanoparticle sizes and the random nature of multiple neutron scattering on powder nanoparticles (see Fig. 7 for a more quantitative analysis).

Note that sp^3 diamond cores of nanoparticles remain intact during fluorination [21], while eliminating nanoparticle shells consisting of sp^2 C modifies the neutron optical potentials of nanoparticles. The data in Fig. 3 confirm this observation. In particular, the efficiency of quasispecular reflection drops, as a function of the neutron wavelength, in a similar way for DNDs and F-DNDs; the overall scaling factor is larger for F-DNDs due to the improvement of the neutron optical potential.

The reflection probability reaches a maximum at a neutron wavelength ∼5 Å for all six curves in Fig. 3, and saturates or even decreases at longer wavelengths. The latter is due to the finite vertical size of the detector. In fact, the total reflection probability continues increasing, as we shall see in Sec. V. However, the angular divergence of neutrons in the sample plane is too large at long wavelengths, and some neutrons do not enter the detector. Nevertheless, we intentionally chose the way of presenting results as in Fig. 3, because it shows the efficiency of quasispecular reflection in the realistic situation of the limited angular divergence of the incident neutron beam and the limited angular acceptance of the instrument downstream. Thus, for a realistic application of quasispecular reflection, the efficiency reaches a maximum at a neutron wavelength corresponding to the maximum intensity of a typical cold neutron beam, for instance, PF1B at ILL [23].

Three pairs of curves in Fig. 3 correspond to three incidence angles (1°, 2°, and 3°); F-DND and DND data are used in each pair. The reflection probability decreases with increasing incidence angle at all wavelengths. This effect can be understood

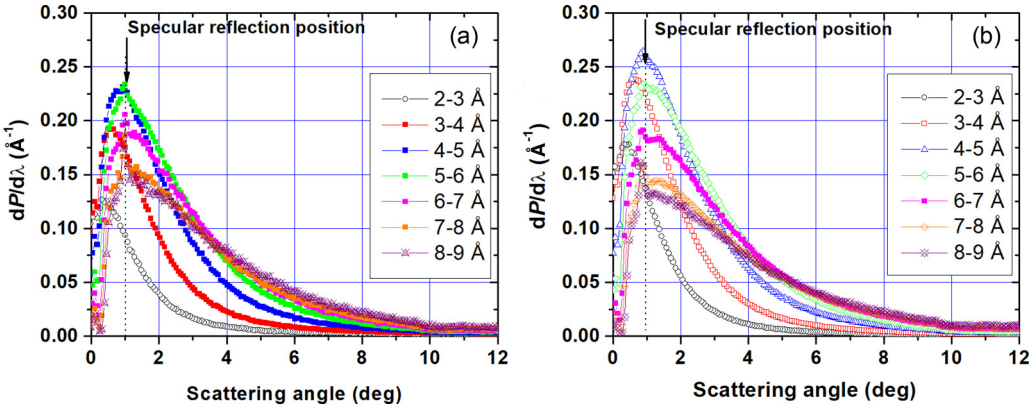

FIG. 4. The differential probability of neutron scattering (vertical axis, per $Å^{-1}$), measured as a function of the scattering angle (horizontal axis, in degrees) from DNDs a) and F-DNDs (b) within the angular acceptance of the D17 detector in the geometry shown in Fig. 1. We integrated the data over the neutron wavelength bands as indicated in the inset and normalized to the total intensity of the incident neutron beam. The neutron incidence angle is 1°.

as follows. Due to the grazing-angle geometry of the setup, the relative change of the wave vector perpendicular to the surface is much larger than the change of the parallel component. The larger the angle of incidence the larger the perpendicular velocity component, and therefore, a smaller probability of reflection.

Finally, we analyze the data within each pair considered above for F-DNDs and DNDs. We compare directly the reflectivity curves near the neutron wavelengths of maximum neutron intensity (4−5 Å), because the angular spread of such scattered neutrons in the sample plane is limited. The reflection efficiency is larger for F-DNDs as expected. At longer wavelengths, measured neutron flux is smaller for F-DNDs; however, this is due to the smaller sizes of F-DNDs after removal of the amorphous carbon as shown in Ref. [21]. A smaller nanoparticle scatters neutrons to larger angles. The integral effect of the nanopowder fluorination to the reflectivity efficiency will be clarified in Sec. V, where the angular distributions of scattered neutrons are taken into account.

Figure 4 presents the results of integrating data over the neutron wavelength bands.

Let us analyze the data measured with F-DNDs corresponding to Fig. 4(b); the data for DNDs in Fig. 4(a) show a similar behavior. As we concluded from the analysis of Fig. 3, the wavelength band of 4−5 Å provides the largest absolute efficiency of quasispecular reflection; also the reflection angle equals the incidence angle. For longer wavelengths, angles shift towards larger values and the angular spread is broader. For shorter wavelengths, angles shift towards smaller values and the angular spread is narrower; however, the observed truncation of the distributions indicates extra neutron losses. We explain these shifts by larger angles of scattering of neutrons with longer wavelengths, and vice versa. The truncation is due to the overall drop of the efficiency of quasispecular reflection at too short wavelengths.

The family of curves in Fig. 3 corresponds to the theoretical curves in Fig. 1 from Ref. [7], where different curves correspond to different angular dependences of scattering on individual nanoparticles. Thus we have proven experimentally that the method of quasispecular reflection of neutrons is sensitive to the angular characteristics of the scattering on individual nanoparticles.

Enhanced scattering at exactly the incidence angle indicates a specular reflection of neutrons from the sample container Si window. It is important at long wavelengths and almost disappears at short wavelength in accordance with simple estimations of the probability of quantum reflection.

As noted already in Ref. [10], the reflection angle and the half dispersion of the scattering angles are approximately equal to the angle of incidence. Here we will analyze this statement in more detail using a data set partially shown in Fig. 4(b) for F-DNDs. Figure 5 illustrates the reflection angle corresponding to the maximum intensity, and Fig. 6 gives the half width of the spread of scattering angles at half height, as a function of the neutron wavelength.

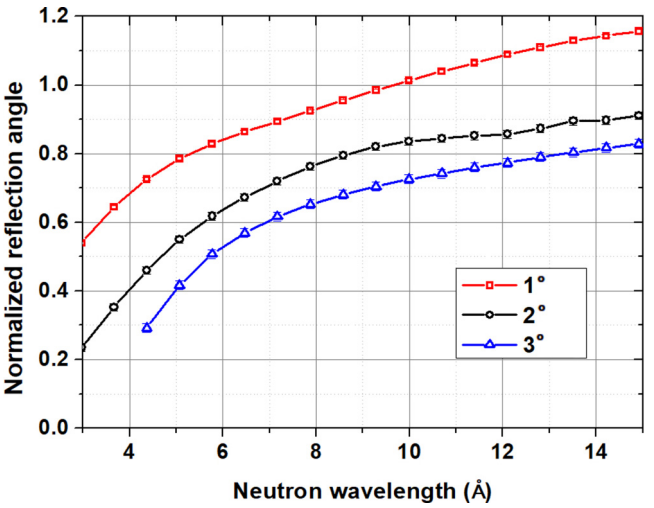

FIG. 5. The angle of quasispecular reflection corresponding to the maximum intensity, in units of the incidence angle, as a function of the neutron wavelength (horizontal axis, in angstroms) for the data shown in Fig. 4(b) for F-DNDs. The incidence angle is 1°, 2°, and 3°. We subtracted the "peak" of specular reflection of neutrons from the sample container Si window.

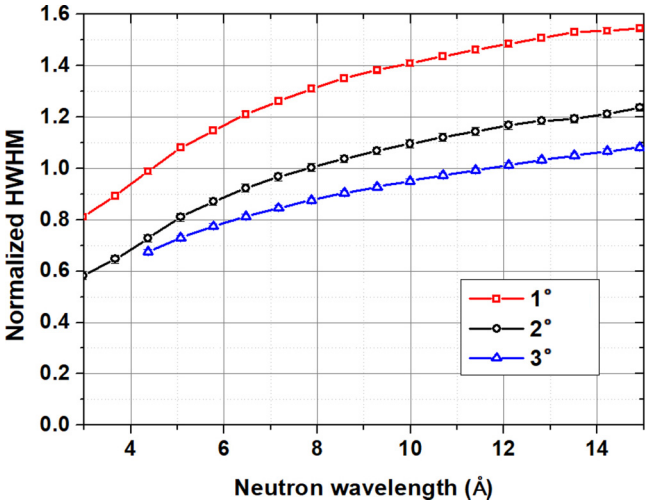

FIG. 6. The half width of the spread of scattering angles, in units of the incidence angle, as a function of the neutron wavelength (horizontal axis, in angstroms) for the data shown in Fig. 4(b) for F-DNDs. The incidence angle is 1°, 2°, and 3°. We subtracted the "peak" of specular reflection of neutrons from the sample container Si window.

The reflection angle and the half width of the spread of scattering angles are approximately equal to the incidence angle for all relevant parameters; the accuracy of this statement can be assessed in Figs. 5 and 6. In particular, for the wavelength of ∼4.5 Å (the maximum quasispecular effect) and the incidence angle of 1° (a typical value), the normalized reflection angle is ∼0.75, and the half dispersion is ∼1.05. For longer wavelengths, the angle of reflection and the half width increase slightly. For shorter wavelengths, these values no longer make sense as quasispecular reflection rapidly disappears. For larger incidence angles, the reflection angle and the half width decrease slightly.

The deviation of the scattering angles from unity, seen in Fig. 5, but not reproduced in Ref. [7], indicate that some assumptions of Ref. [7] are not valid in our case; in particular the number of scattering events in the experiment is not "infinite"; also interference effects and specific loss mechanisms are absent in the theory.

V. SIMULATION

Precise calculation of the neutron propagation in a DND (F-DND) powder is a complex problem. However, the first model of Monte Carlo trajectory simulation of neutron scattering on independent monodispersed structureless nanoparticles, as described in [14,15], already provided a reasonable description of the data at neutron wavelengths above the diamond Bragg cutoff, with an accuracy of ∼20%−30%. Further developments took into account the size distribution, chemical composition, and structure of nanoparticles; free parameters of the model are adjusted using neutron, x-ray, and other data. Although the development of this model [24] is still ongoing, the calculation of relative effects, for example, related to the fluorination of nanoparticles, is rather straightforward.

The family of curves in Fig. 7(a) corresponds to the theoretical curves in Fig. 2 from Ref. [7], where different curves correspond to different angular dependences of scattering on individual nanoparticles. Thus again, we have proven experimentally that the method of quasispecular reflection of neutrons is sensitive to the angular characteristics of the scattering on individual nanoparticles. As clear from Fig. 7(a), the total probability of quasispecular reflection of neutrons from the open surface of F-DND powder reaches ∼70% at

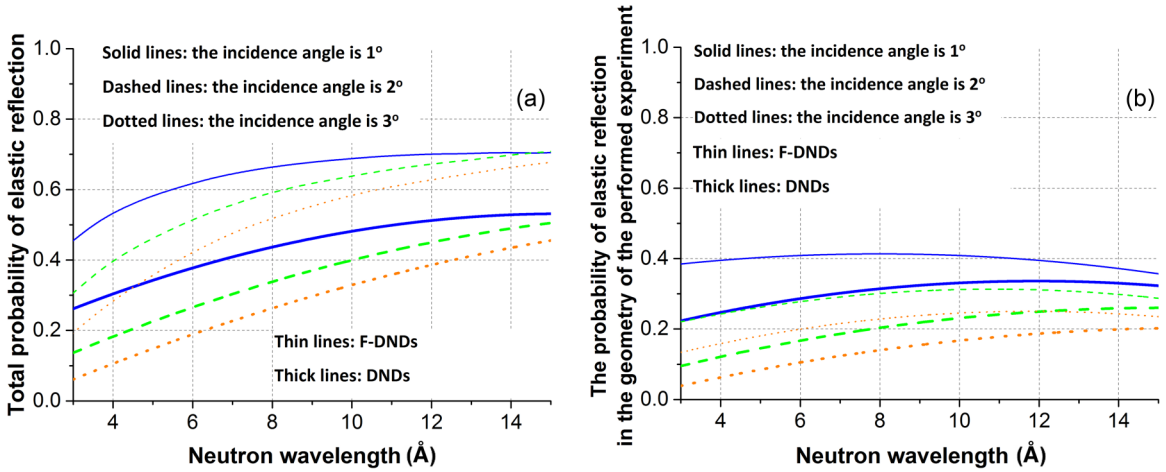

FIG. 7. (a). The simulated total probability of elastic reflection of neutrons at different angles of incidence on the layers of F-DND and DND, as a function of the neutron wavelength. We do not take into account the window on the powder surface and assume that the thickness of the layer is infinitely large. The total effect of hydrogen is small for F-DNDs (1%−2%). Although it is large for DNDs, its contribution to the quasispecular directions is also small (2%−3% within the detector solid angle). Thin lines correspond to F-DND. Thick lines indicate the results for DNDs. Solid, dashed, and dotted lines, respectively, show the results for the neutron incidence angles of 1°, 2°, 3°. The thickness of the lines is approximately equal to the statistical accuracy of the simulations. In these simulations, we do not take into account the diffraction of neutrons on the diamond lattice (important at the shortest wavelengths) and the interference effects associated with neutron scattering on many nanoparticles (important at the longest wavelengths). (b). Here, in contrast to (a), we take into account a limited angular size of the detector and neutron losses in the Si window.

long neutron wavelengths. At neutron wavelengths of 4−6 Å (typical cold neutron beams) and incidence angles 1°−2°, the total probability of quasispecular reflection is 40%−60% (or 45%−65%, taking into account interference effects).

This reflection probability corresponds to the following hypothesis about the angular dependence of individual scatterings:

$$I(\vartheta) = \frac{1}{\pi} \frac{\nu \vartheta_{\text{eff}}^{\nu}}{\left(\vartheta_{\text{eff}}^2 + \vartheta\right)^{1+\nu}}, \tag{6}$$

where $I(\vartheta)$ is the intensity of the individual scattering as a function of the scattering angle, and ϑ_{eff} is the effective small-angle scattering angle, while the parameter ν is approximately equal to unity as follows from the comparison of the measured probabilities and Fig. 2 in Ref. [7].

Such an angular dependence of the neutron scattering probability on a single nanoparticle (a quadratic asymptotic) is in good agreement with the expected dependence [see Eq. (4)], which is a good test of the correctness of the results obtained.

To design any particular configuration involving nanodiamond reflectors, one should take into account the angular distributions of incident and reflected neutrons; they should be sufficiently broad. In the case of significant angular collimations, the intensities will drop. However, in some cases (extraction of cold neutrons from neutron sources, focusing devices, shaping devices to avoid the direct line of sight of the source of radiation) angular constraints might be less important. These angular dependences can be evaluated by extrapolating (interpolating) our experimental results, using computer simulation or using general analytical formulas [7].

Finally, we want to draw the reader's attention to a small "resonance" apparent in the raw data in Fig. 3. At the neutron wavelength ∼5 Å, one can see the enhancement of quasispecular reflection not reproduced in the simulation shown in Fig. 7. This is mainly due to the interference of two scattering amplitudes: on the nanoparticle optical potential and on the diamond lattice. While a small change in the size of the nanoparticle does not significantly change the mean probability of quasispecular reflection, it strongly changes the Bragg cutoff. Here, we do not explicitly take into account the diamond particle lattice in the simulations shown in Fig. 7 (as not relevant to the subject of this work) but plan to perform a dedicated study in future. In particular, it would be useful to carry out measurements with nanoparticles of larger size.

VI. CONCLUSION

We studied the quasispecular reflection of cold neutrons from powders of raw and fluorinated detonation nanodiamonds. We had not treated the powder *in situ*, thus simulating typical conditions in possible applications of the method. As expected, fluorination, which had removed hydrogen and amorphous sp^2 carbon from the surface of the nanoparticles, increased the probability of quasispecular reflection. The total probability increases to ∼70% at long wavelengths (10−15 Å) and became equal to 45%−65% at wavelengths 4−6 Å corresponding to the maximum intensity in typical cold neutron beams.

We showed quantitatively that in a broad range of initial parameters relevant for quasispecular reflection of cold neutrons, the reflection angle and the half width of the spread of scattering angles are approximately equal to the angle of incidence.

This method is an alternative tool for experiments with cold neutrons. It can be used for focusing and delivery of neutrons, and is thus complementary to supermirrors [25], at certain conditions. It might serve for designing and building more efficient neutron facilities and sources.

ACKNOWLEDGMENTS

The measurements and sample characterization were performed on the D17 [22], GRANIT [26], and PF1B [23] instruments at ILL. The authors are grateful to the instrument responsibles and our GRANIT and SLON collaborators, for their help during the measurements and useful discussions.

[1] P. Sheng, *Scattering and Localization of Classical Waves in Random Media* (World Scientific, Singapore, 1990).
[2] J. Schelten and W. Shmatz, J. Appl. Crystal. **13**, 385 (1980).
[3] S. V. Mallev and B. P. Toperverg, JETP Lett. **51**, 158 (1980).
[4] L. A. Feigin and D. I. Svergun, *Structure Analysis by Small-Angle X-Ray and Neutron Scattering* (Plenum Press, New York, 1987).
[5] T. M. Sabine and W. K. Bertram, Acta Crystallogr. **55**, 500 (1999).
[6] A. Ishimaru, *Wave Propagation and Scattering in Random Media* (Wiley-IEEE Press, Piscataway, NJ, 1999).
[7] V. S. Remizovich, JETP **60**, 290 (1984).
[8] P. J. de Carli and J. C. Jameieson, Science **133**, 1821 (1961).
[9] A. E. Aleksenskii, M. V. Baidakova, A. Yu. Vul', and V. I. Siklitskii, Phys. Solid State **41**, 668 (1999).
[10] V. V. Nesvizhevsky, R. Cubitt, E. V. Lychagin, A. Yu. Muzychka, G. V. Nekhaev, G. Pignol, K. V. Protasov, and A. V. Strelkov, Materials **3**, 1768 (2010).
[11] R. Cubitt, E. V. Lychagin, A. Y. Muzychka, G. V. Nekhaev, V. V. Nesvizhevsky, G. Pignol, K. V. Protasov, and A. V. Strelkov, Nucl. Instrum. Methods Phys. Res., Sect. A **622**, 182 (2010).
[12] V. V. Nesvizhevsky, Phys. At. Nucl. **65**, 400 (2002).
[13] V. A. Artem'ev, At. Energy **101**, 901 (2006).
[14] V. V. Nesvizhevsky, E. V. Lychagin, A. Yu. Muzychka, A. V. Strelkov, G. Pignol, and K. V. Protasov, Nucl. Instrum. Methods Phys. Res., Sect. A **595**, 631 (2008).
[15] E. V. Lychagin, A. Yu. Muzychka, V. V. Nesvizhevsky, G. Pignol, K. V. Protasov, and A. V. Strelkov, Phys. Lett. B **679**, 186 (2009).
[16] E. V. Lychagin, A. Yu. Muzychka, and V. V. Nesvizhevsky, Nano-structured reflectors for slow neutrons, in *New Developments in Low Energy Physics*, edited by M. N. Tao Zoeng (Nova, New York, 2012).

[17] V. K. Ignatovich and V. V. Nesvizhevsky, At. Energy **116**, 132 (2014).
[18] E. V. Lychagin, A. Yu. Muzychka, V. V. Nesvizhevsky, G. V. Nekhaev, G. Pignol, K. V. Protasov, and A. V. Strelkov, Nucl. Instrum. Methods Phys. Res., Sect. A **611**, 302 (2009).
[19] V. V. Nesvizhevsky, Rev. Mex. Fis. **57**, 1 (2011).
[20] A. R. Krylov, E. V. Lychagin, A. Yu. Muzychka, V. V. Nesvizhevsky, G. V. Nekhaev, A. V. Strelkov, and A. S. Ivanov, Crystallogr. Rep. **56**, 1186 (2011).
[21] V. V. Nesvizhevsky, U. Koester, M. Dubois, N. Batisse, L. Frezet, A. Bosak, L. Gines, and O. Williams, Carbon **130**, 799 (2018).
[22] R. Cubitt and G. Fragneto, Appl. Phys. A **74**, s329 (2002).
[23] H. Abele, D. Dubbers, H. Hase, M. Klein, A. Knopfler, M. Kreuz, T. Lauer, B. Markisch, D. Mund, V. V. Nesvizhevsky, A. K. Petukhov, C. Schmidt, M. Shumann, and T. Soldner, Nucl. Instrum. Methods Phys. Res., Sect. A **562**, 407 (2006).
[24] A. Yu. Nezvanov *et al.* (unpublished).
[25] F. Mezei, Commun. Phys. **1**, 81 (1976).
[26] S. Baessler, M. Beau, M. Kreuz, V. N. Kurlov, V. V. Nesvizhevsky, G. Pignol, K. V. Protasov, F. Vezzu, and A. Yu. Voronin, C. R. Phys. **12**, 707 (2011).